Atomic Layer Deposition of Dielectric Overlayers for Enhancing the Optical Properties and Chemical Stability of Plasmonic Nanoholes

Hyungsoon Im, Nathan C. Lindquist, Antoine Lesuffleur, and Sang-Hyun Oh*

Laboratory of Nanostructures and Biosensing, Department of Electrical and Computer Engineering, University of Minnesota, Twin Cities, 200 Union Street S.E., Minneapolis, Minnesota 55455

ABSTRACT Fabricating plasmonic nanostructures with robust optical and chemical properties remains a challenging task, especially with silver, which has superior optical properties but poor environmental stability. In this work, conformal atomic layer deposition (ALD) of thin alumina overlayers is used to precisely tune the optical transmission properties of periodic nanohole arrays made in gold and silver films. Experiments and computer simulations confirm that ALD overlayers with optimized thicknesses tune and enhance the transmitted intensity due to refractive index matching effects and by modifying the dielectric properties of each nanohole. Furthermore, encapsulating silver nanohole arrays with thin alumina overlayers protects the patterned surfaces against unwanted oxidation and contamination. The ability to precisely tune the optical properties while simultaneously providing robust chemical stability can benefit a broad range of applications, including biosensing and fluorescence imaging.

KEYWORDS: extraordinary optical transmission · periodic nanohole arrays · atomic layer deposition · plasmonic biosensing · device encapsulation.

Nanostructures made from noble metals such as gold or silver can harness electromagnetic surface waves known as surface plasmons (SP), which are electron density fluctuations that propagate along the surface of the metal.[1] Because of the strong coupling between photons and the conduction electron plasma, the SP is confined to within ~100 nm of the metal-dielectric interface in the form of an exponentially decaying evanescent field. By harnessing these unique qualities of SP waves, plasmonic nanostructures can squeeze light into nanometer-scale volumes, generating large field enhancements, and showing promise for applications in sensing, spectroscopy, photovoltaics and data storage.[2−6] In particular, Ebbesen's discovery of the SP-mediated extraordinary optical transmission (EOT) effect has generated intense interest in the emerging field of plasmonics.[7,8]

Since SP waves exist within ~100 nm of the metal surface, their properties can be sharply modulated by local refractive index changes due to the adsorption of a thin film of molecules, providing the basis for surface plasmon resonance (SPR) biosensing. By virtue of the SP-mediated EOT effect, periodic nanohole arrays can also function as SPR biosensors, operating in a colinear transmission imaging mode.[9−17] In these nanohole SPR imaging systems, the source, sample and detectors are all aligned along the same optical axis, allowing high-resolution SPR imaging.[18] The development of biosensors based on the EOT effect requires systematic investigations of how the thickness and spatial distribution of a thin adsorbed film affects the optical transmission properties. A simple method for tuning the local refractive index in the vicinity of the nanoholes can provide the design freedom to optimize the EOT effect.

The effects of using different metals are also of importance for plasmonics.[19−22] Within the visible spectrum, silver-based plasmonic devices exhibit better intrinsic performance—for example, longer SP propagation lengths and higher sensitivity for biosensing—than devices made from gold, copper, or aluminum. Nevertheless, many plasmonic devices, including the majority of biosensors, are made with gold. One of the reasons lies in the poor chemical stability of silver: it oxidizes readily in air and easily forms an Ag_2S contaminating adlayer, resulting in unstable chemical properties. In comparison, gold is inert, has been more widely used as standard substrates for self-assembled monolayer chemistry, and, unlike silver,[23] is not toxic to cells. In many applications where interfacing with biological materials is not required, for example,

*Address correspondence to sang@umn.edu.

Received for review December 16, 2009 and accepted January 26, 2010.

Published online February 4, 2010.
10.1021/nn901842r

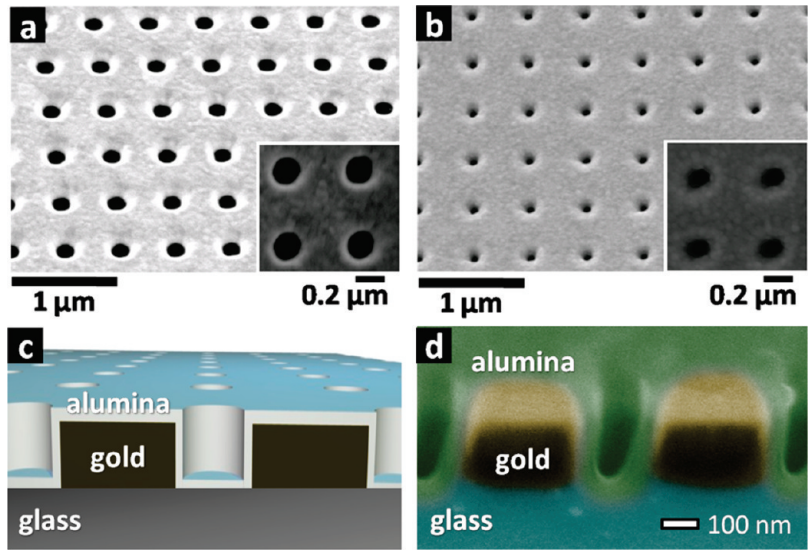

Figure 1. A SEM image of nanohole arrays in gold film on a glass substrate (a) before and (b) after ALD of a 40 nm thick alumina overlayer. The insets to panels a and b show enlarged images of the nanoholes; (c) a cross-sectional schematic of a nanohole array with an alumina overlayer deposited with ALD; (d) a cross-sectional SEM image of a nanohole array with a 40 nm ALD-grown alumina overlayer.

as electrodes for plasmonic solar cells, silver has been used because of its lower cost, better optical properties, and its better adhesion to glass substrates,[24,25] though stability remains an issue. Therefore, a broad range of applications can benefit by developing a simple method that can harness the increased plasmonic performance of silver while circumventing its poor chemical stability. A conformal atomic layer deposition (ALD) of a dielectric overlayer, such as alumina (Al_2O_3) or silicon dioxide (SiO_2), on three-dimensional (3-D) nanostructures can provide a solution that is generally applicable.

In this work, we use the ALD growth of alumina overlayers to characterize the EOT effect through nanohole arrays in gold and silver films while simultaneously protecting the surfaces against oxidation and contamination. Interestingly, EOT intensity is enhanced with the addition of the alumina overlayers, which is explored with extensive 3-D computer simulations. Finally, it is shown that adding a ~20 nm thick alumina overlayer does not degrade the molecular detection sensitivity of silver periodic nanohole arrays while simultaneously providing protection even under harsh oxidizing conditions.

RESULTS AND DISCUSSION

Nanohole arrays made in a metallic film on a glass substrate with and without Al_2O_3 overlayers are shown in Figure 1. The nanohole arrays were milled using an FEI dual-beam focused ion beam (FIB). Nanoholes were milled through a 200-nm-thick gold (with a 5 nm chromium (Cr) adhesion layer) or silver (without a Cr adhesion layer) film on a glass substrate. Each array consisted of 16 × 16 nanoholes with a periodicity of 500 nm and a hole diameter of 180 nm (Figure 1a). For encapsulation (Figure 1b), ALD of thin Al_2O_3 overlayers was used. Alumina is deposited conformally by ALD, covering the flat metal areas as well as the sidewalls and bottoms of the nanoholes, sketched in Figure 1c, and confirmed in a cross-sectional scanning electron microscope (SEM) image (Figure 1d).

The ALD technique utilizes self-limiting chemical reactions to enable conformal deposition of compound thin films with subnanometer thickness resolution.[26,27] In particular, alumina can act as an excellent barrier against gas diffusion and is thus suitable for device encapsulation.[28] Due to these desirable properties, ALD-deposited alumina has also been used to characterize the localized surface plasmon resonance (LSPR) of silver nanoparticles and to increase the stability of patterned silver films for surface-enhanced Raman spectroscopy.[29,30]

Figure 2 shows how the transmission spectra of both gold and silver nanohole arrays (180 nm hole diameter and 500 nm periodicity) change *versus* Al_2O_3 thicknesses. When light is incident on a noble metal film perforated with a periodic array of subwavelength nanoholes, the EOT effect manifests itself as a series of intense peaks in the optical transmission spectra that are stronger than predicted by classical diffraction theory. The enhancement occurs through the excitation of SP waves in this nanostructure,[7,31,32] wherein the periodic nanohole array acts as a two-dimensional diffraction grating that converts incident photons into SP waves. The peak transmission wavelengths for normally incident light are approximated by

$$\lambda_{peak} = \frac{a_0}{\sqrt{i^2 + j^2}} \sqrt{\frac{\varepsilon_m \varepsilon_d}{\varepsilon_m + \varepsilon_d}} \quad (1)$$

where a_0 is the periodicity of the nanohole array, i and

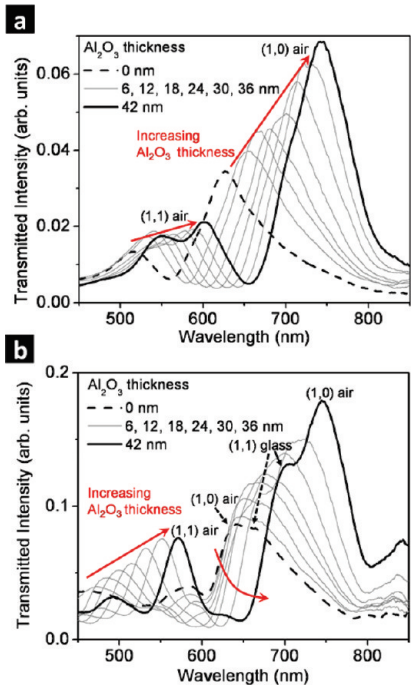

Figure 2. Sequence of transmission spectra through the same 16 × 16 nanohole array as the thickness of the ALD-grown Al_2O_3 overlayer increases from 0 to 42 nm at 6 nm intervals. The diameter and periodicity of nanohole is 180 and 500 nm, respectively. The nanoholes were milled through (a) gold and (b) silver films.

j are the grating orders, and ϵ_m and ϵ_d are the dielectric constants of the metal and dielectric, respectively. Measured transmission spectra show red shifts from the λ_{peak} values predicted in eq 1 because of Fano interference between the direct transmission through the holes and the excitation of the surface modes.[33]

The optical transmission through the nanohole array in a gold film shows two significant peaks that correspond to the (1,0) and (1,1) resonances at the gold-air interface from eq 1. The resonance peaks at the gold−glass interface are dampened due to the presence of a 5 nm Cr adhesion layer. In the case of silver, the observed resonances are more complicated since there is no Cr adhesion layer. There are four main components: the (1,0) and (1,1) resonances at the silver−glass interface and the (1,0) and (1,1) resonances at the silver−air interface. For both samples, however, the metal−air transmission peaks red-shift and their intensity increases as the thickness of the Al_2O_3 overlayer increases from 0 up to 42 nm. The spectral shifts are mainly due to the refractive index response of the SPs. In a simplified model, the effective refractive index n_{eff} seen by the SP waves can be approximately calculated as[34]

$$n_{eff} = n_{bulk} + (n_{layer} - n_{bulk})(1 - \exp(-2d/l)) \quad (2)$$

where n_{layer} and n_{bulk} are the refractive indices of a thin layer deposited on the metal and of the surrounding bulk material, respectively, *d* is the thickness of the deposited layer, and *l* is the decay length of SP evanescent field perpendicular to the surface. Although this equation is not directly applicable to our 3-D nanohole geometry, it can be seen that as the thickness of the Al_2O_3 overlayer increases, n_{eff} increases as n_{bulk} is smaller than n_{layer}. In our case, n_{bulk} is air and n_{layer} is Al_2O_3, increasing n_{eff} and red-shifting λ_{peak}. Therefore, the ALD growth of a dielectric layer, with its ultrafine thickness resolution, can precisely tune the plasmon resonance of metallic nanostructures. Additionally, as the peaks red-shift, the transmitted light intensity also increases, shown in Figure 2. This is partly due to decreased SP damping losses at longer wavelengths, demonstrated by Przybilla *et al.*[35] In that work, when the period of the array was enlarged to position the transmission peak at longer wavelengths, they observed an increase in the optical transmission intensity due to the reduced SP damping. Although the geometry of our system is different because of the 3-D conformal deposition of Al_2O_3 inside each nanohole and on the top metal surface, the reduced SP damping at longer wavelengths also plays a role. In addition, as the effective hole size is increased due to filling the hole with a higher index Al_2O_3, the waveguide-type attenuation in the subwavelength holes decreases, boosting the transmission. Furthermore, index-matching effects between both sides of the film, that is, making an asymmetric system (air−metal−glass) into an effectively symmetric one (air−alumina−metal−glass) at a certain Al_2O_3 thickness, have also been shown to increase the transmission efficiency.[36]

To confirm these underlying mechanisms for enhancing the EOT effect, the experimental data were compared with full 3-D finite-difference time-domain (FDTD) simulations. Figure 3a shows color maps consisting of experimental transmission spectra (similar data to Figure 2) measured after each consecutive deposition of 6 nm of Al_2O_3 on the same sample (gold). Figure 3b shows color maps constructed from 3-D FDTD simulations for every 10 nm of conformal alumina deposition. In the color maps, the positions of the (1,0) and (1,1) resonance maxima and the transmission minima are shown with white dashed lines. It is seen that all of the maxima and minima are red-shifted as the thickness of Al_2O_3 layer increases. Also, the intensity of each peak increases up to a factor of about 5 until the Al_2O_3 layer reaches a certain thickness. Similar trends are observed from silver nanohole arrays in Figure 3c,d. The positions of the transmission peaks in the spectra from the experimental results match well (within 10 nm) with the FDTD calculations, and the trends in wavelength shifts and intensity changes are consistent. The thickness of the Al_2O_3 overlayer where the maximum peak intensity was achieved experimentally (~100 nm) is different from that of FDTD calculations (~70 nm). The difference is likely to come from the imperfections in fabrication such as the rounded edges of the FIB-

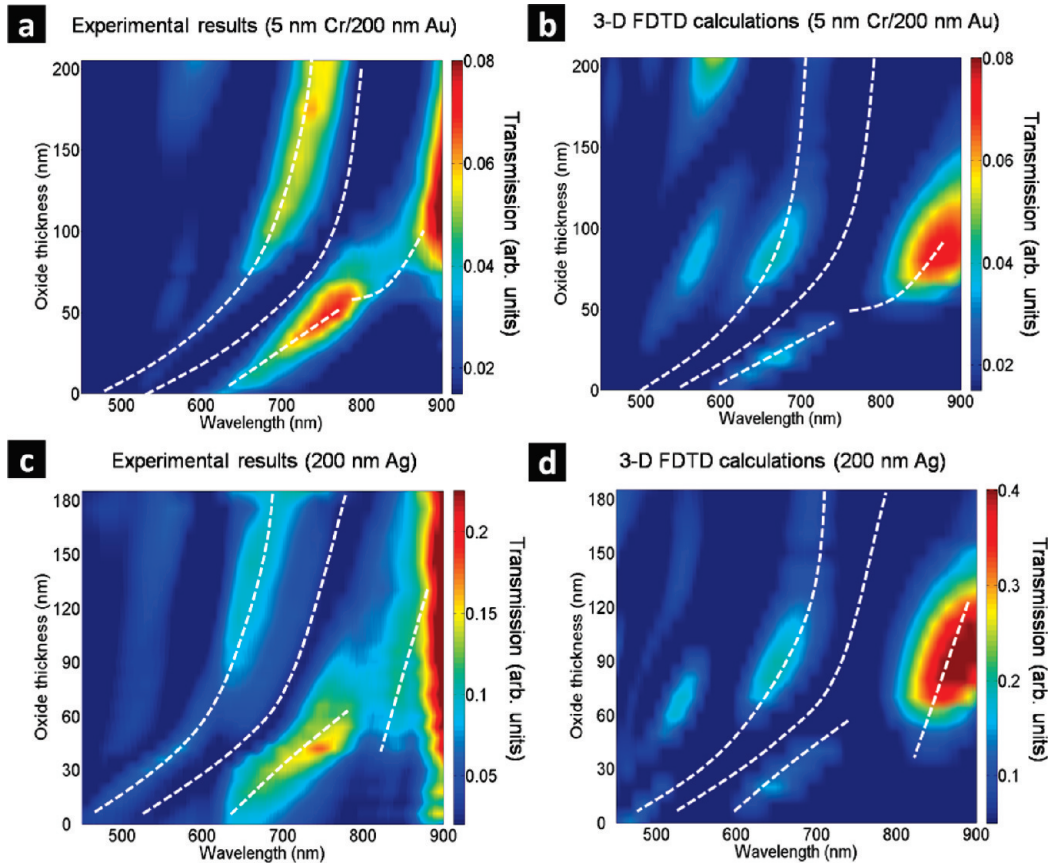

Figure 3. Color maps of the transmission spectra of a 16 × 16 nanohole array with a 180 nm hole diameter and a 500 nm periodicity. (a) Experimental results of a nanohole array made in a 200 nm thick gold film as the Al_2O_3 thickness increases from 0 to 205 nm; (b) 3-D FDTD calculations with the same structure as panel a; (c) Experimental results with the nanohole array made in a 200 nm silver film as the Al_2O_3 thickness increases from 0 to 185 nm; (d) 3-D FDTD calculations with the same structure as panel c. Dashed lines track the positions of the (1,0) and (1,1) resonance peaks as well as transmission minima.

patterned holes (Figure 1d) as well as the roughness of metal surface.

Figure 4 shows the spectral shifts of the $(1,1)_{air}$ resonance peaks of Ag and Au nanohole arrays as a function of increasing Al_2O_3 overlayer thickness. The $(1,0)_{air}$ resonance peak was not tracked because of the wavelength range limits of our spectrometer. Beyond ~100 nm thickness, comparable to the decay length of the SP evanescent field, the spectral red-shift saturates. In the linear region, where the alumina overlayer thickness is less than 50 nm, the spectral shifts for both Ag and Au nanohole arrays are linearly proportional to the oxide thickness, and the slope of the change, corresponding to the detection sensitivity of the array, is unchanged by the alumina overlayer. This experiment shows that an overlayer thickness of up to 50 nm does not degrade the sensitivity for detecting the subsequent deposition of an additional 6 nm-thick alumina layer. Increasing the overlayer thickness, however, gradually reduces the probing range, and the detection sensitivity is sharply degraded. The spectral red-shift and subsequent saturation were also observed in a recent work by Stewart *et al.*[37] who used layer-by-layer assembly to deposit polyelectrolyte on plasmonic crystals and studied how to optimize their molecular detection sensitivity.

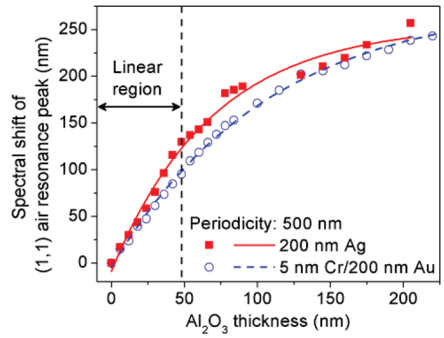

Figure 4. As the thickness of the Al_2O_3 overlayer increases from 0 to 205 nm, the $(1,1)_{air}$ peaks of the Ag and Au nanohole arrays red-shift. The periodicity is 500 nm and the hole diameter is 180 nm for both Ag and Au nanohole arrays. A 5 nm Cr adhesion layer was used only for the Au film. Experimental results are shown as squares (Ag) and circles (Au), and the data are fit with exponentially saturating curves. The shift is approximately linear with Al_2O_3 thicknesses ranging from 0 to 48 nm.

To provide insights into the role of effectively matching the refractive indices on the top and bottom sides of the metal film by the addition of the ALD overlayers, the full electromagnetic field distributions of each nanohole were calculated with 3-D FDTD simulations. In these simulations, the nanohole arrays were 180 nm

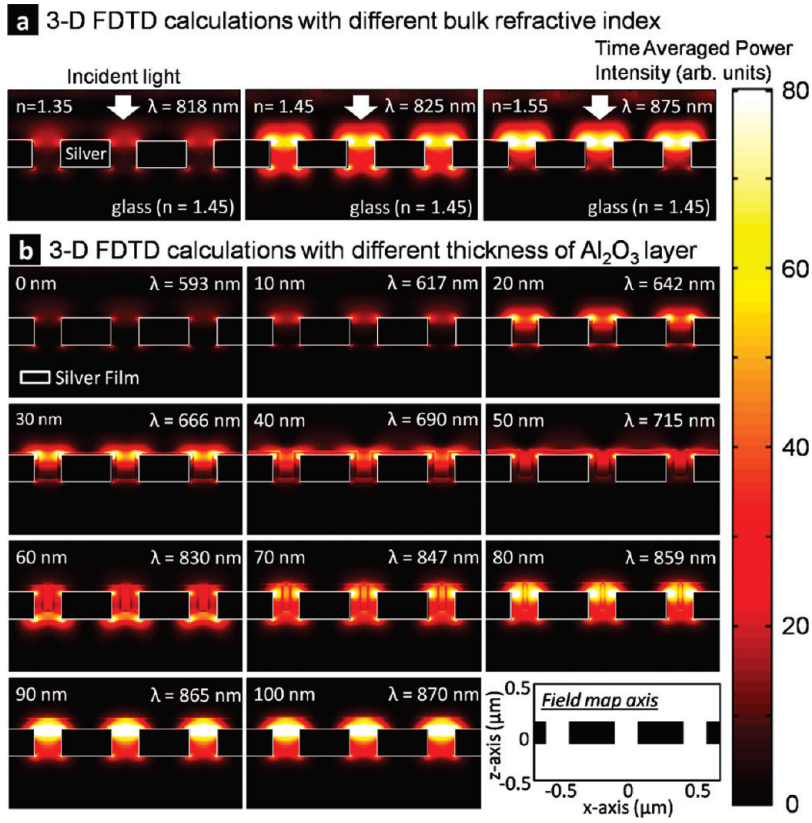

Figure 5. (a) 3-D FDTD simulation results showing the time-averaged surface plasmon (SP) field intensity for different bulk refractive indices changing from 1.35 to 1.55. The refractive index of the glass substrate is 1.45, giving maximum transmission when matched to the bulk. (b) Different thicknesses of a conformal Al_2O_3 overlayer ranging from 0 to 100 nm. The nanoholes have a diameter of 180 nm and have a 500 nm periodicity in a 200 nm thick silver film. Light is incident from the top. The field maps are calculated at the resonant peak wavelengths indicated in each panel.

in diameter, with a periodicity of 500 nm, with a silver film thickness of 200 nm. Figure 5a shows the time-averaged EM field intensity in the vicinity of the periodic silver nanohole arrays with different bulk refractive indices over the nanohole array varying from 1.35 to 1.55. The cross-sectional images confirm that the maximum transmitted intensity and maximum output field intensity occurs when the refractive index of the bulk medium above and inside each nanohole matches that of the glass substrate ($n = 1.45$). This effect was also demonstrated by Krishnan *et al.*[36] who showed that the optical transmission through symmetric hole arrays, wherein the energies of the SP modes on both sides of the film are equal, is enhanced by a factor of ~10 over asymmetric arrays.

Figure 5b shows the EM field power distributions with different alumina thicknesses from 0 to 100 nm on the silver nanohole arrays. In our case, the glass substrate has a refractive index of 1.45 while the alumina film has an index of 1.65. Although the 3-D geometry of the ALD overlayer does not make a completely symmetric geometry, it is expected that the effective index of the alumina overlayer seen by the SP waves, from eq 1, can closely match the refractive index of the glass substrate for a certain alumina thickness. Simply comparing the EM field power distributions in Figure 5b with those in Figure 5a, it can be seen that the enhanced transmitted intensity due to effective refractive index matching occurs at an Al_2O_3 thickness between 60 and 70 nm. Therefore, the ALD overlayer can be used to shift the EOT spectrum and increase the optical transmission of plasmonic nanoholes in a precisely controlled manner, which will be valuable for biochemical sensing and photonics as well as for understanding the various mechanisms involved in the EOT effect. In particular, the increased optical transmission can improve SPR imaging systems, which is often dominated by shot noise.[38]

Besides enhancing plasmon resonances and providing tunability, the conformal deposition of Al_2O_3 overlayers simultaneously acts as an encapsulation layer to protect silver nanohole arrays against unwanted oxidation or contamination. It has been reported that even a few nanometers of Al_2O_3 layer deposited by ALD is sufficient for blocking water vapor transmission through the layer.[28,39] For robust protection against unwanted oxidation, a thicker oxide is more desirable. On the other hand, to maintain sensitivity to molecules binding on the surface, a thinner overlayer is needed. As seen in Figure 4, the spectral response remained linear to additional thin layers with a total thickness below 50 nm. Therefore, a 20 nm Al_2O_3 overlayer, which does not sacrifice the detection sensitivity and is at the lower

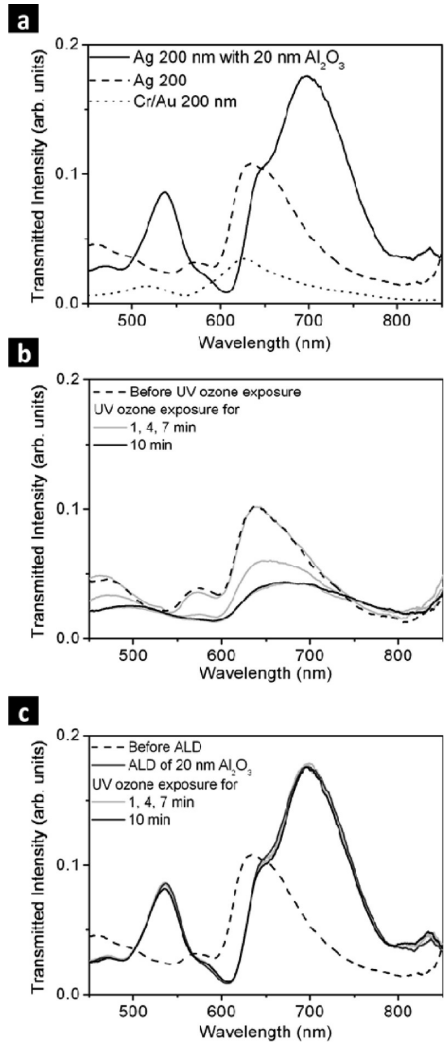

Figure 6. (a) Comparison of transmission spectra through nanohole arrays made in a 200 nm thick silver film (dashed line), a 200/5 nm thick gold/chromium (dotted line) film, and with a 20 nm Al_2O_3 layer deposited on the silver sample (solid line). The nanohole arrays have a diameter of 180 nm and have a 500 nm periodicity. (b) Transmission spectra change as a nanohole array made in a silver film is exposed to UV ozone for 1, 4, 7, and 10 min without a protective Al_2O_3 overlayer and (c) with a 20 nm protective Al_2O_3 overlayer.

end as a gas diffuse barrier, was chosen to fulfill both requirements, and its resistance against oxidation was tested.

Figure 6a shows transmission spectra for three types of nanohole arrays: made in a 200 nm thick gold film with a 5 nm-thick Cr adhesion layer; a 200 nm thick silver film; and a 200 nm thick silver film with a 20 nm-thick protective Al_2O_3 overlayer. The nanohole array made in the silver film, which does not have a Cr adhesion layer, shows higher transmission intensity than the array made in gold with a Cr adhesion layer films with the same nominal nanohole parameters. The transmission through the silver nanohole array is further enhanced following the deposition of a 20 nm-thick Al_2O_3 overlayer. The Al_2O_3 layer was deposited at 50 °C to prevent the possibility of silver oxide formation inside the ALD chamber due to trace amounts of water vapor.[29]

Following the initial measurements of the EOT spectra, all samples were simultaneously exposed to the oxidizing environment inside a UV−ozone chamber, and their individual optical transmission spectra were recorded after 1, 4, 7, and 10 min of oxidation. The EOT spectrum of the gold nanohole array did not show any measurable change after 10 min of oxidation (data not shown). On the other hand, the nanohole array milled in a bare silver film shows a dramatic reduction in the optical transmission intensity as well as broadened peak widths, shown in Figure 6b, which was caused by the formation of a surface oxide layer. The silver nanohole array that was encapsulated with 20 nm of alumina did not show any noticeable change in the transmission spectra, shown in Figure 6c. This result confirms that an Al_2O_3 overlayer acts as a good passivation layer for preventing the oxidation of silver. The exact thickness of the alumina overlayer depends on the specific applications, weighing whether oxidation protection or maintaining sensitivity to surface events is more important.

Simple ALD encapsulation using alumina (Al_2O_3), silicon dioxide (SiO_2), or hafnium oxide (HfO_2) overlayers can be used for other metals such as copper or aluminum, to tune their optical properties and protect the surface from oxidation. The surface of ALD-encapsulated silver nanohole arrays or other 3-D plasmonic devices can be subsequently functionalized by using a self-assembled monolayer such as 3-aminopropyl triethoxysilane (APTES) for biosensing.[40] Also, plasmonic nanostructures coated with ALD overlayers can be used to precisely control the coupling between quantum emitters and the SP waves[41] as well as fluorescence quenching.

CONCLUSION

The EOT effect through gold and silver nanohole arrays was systematically characterized as a thin Al_2O_3 overlayer was sequentially deposited by ALD. As the resonance wavelength is red-shifted by the deposition of an Al_2O_3 overlayer, the transmission intensity increases because of the lower SP damping losses, increased cutoff wavelength by conformally filling nanoholes with higher index Al_2O_3, and effective refractive index matching effects between both sides of the metal film. It was experimentally shown that a 50-nm-thick alumina overlayer did not degrade the detection sensitivity of nanohole sensors, thus allowing them to function as biochemical sensors. Furthermore, the Al_2O_3 overlayer protects silver surfaces against the growth of adventitious oxide while acting as a substrate over which to attach other molecules for biosensing. The ALD encapsulation technique using a thin alumina, SiO_2

or HfO_2 overlayer can be easily applied to metallic nanostructures made from Au, Ag, Cu, or Al to precisely tune their plasmonic resonances while protecting their surfaces. In addition, the ALD overlayer can be coupled with high-throughput nanofabrication techniques such as template stripping,[42] soft interference lithography,[43] and nanosphere lithography[44,45] to generate a broad range of patterned plasmonic nanostructures with improved optical properties and stable functional surfaces.

METHODS

Atomic Layer Deposition (ALD). Al_2O_3 overlayer films were deposited by ALD on the metallic nanohole arrays. Trimethylaluminum (TMA) and water vapor were sequentially pulsed through the reaction chamber. N_2 gas was used to purge the chamber after injecting each precursor. The operating temperature was 250 °C for depositing Al_2O_3 films on a gold substrate. In the case of silver substrates, Al_2O_3 films were deposited at 50 °C to minimize the oxidation of a silver film during the ALD process.[29] The transmission spectra were measured immediately after each deposition to minimize exposure time of the sample to air.

Computer Simulations. 3-D finite-difference time-domain (FDTD) simulations were performed using Fullwave (RSoft Design Group). A nonuniform mesh was used, which had a nominal size of 5 nm and edge-interface grid size of 1 nm and which incorporated at least 20 grid points within the thin ALD layers. The refractive indices of the glass substrate and alumina overlayers were set to 1.45 and 1.65, respectively. Periodic boundary conditions were used to simulate an infinite array of periodic nanoholes. A plane wave was incident from the top (ALD) side of the nanohole array, pulsed in time with a Gaussian envelope to have a spectral width of ~700 nm and centered at 500 nm. The transmitted power was recorded, and a Fourier transform was calculated to obtain the simulated spectral response of the system. The complex dielectric constants of gold and silver were modeled as having a Drude−Lorentz dispersion response, fitted to Johnson and Christy experimental values.[46]

Acknowledgment. We thank T.W. Ebbesen and M.A. Pelton for reading our manuscript and providing helpful comments. S.-H.O. acknowledges support from ACS Petroleum Research Fund's Doctoral New Investigator Award and from Minnesota Supercomputing Institute. H.I. and N.C.L. acknowledge 3M Science and Technology Fellowship and UMN Doctoral Dissertation Fellowship, respectively. Device fabrication was performed at the UMN Nanofabrication Center, which receives partial support from NSF NNIN.

REFERENCES AND NOTES

1. Ritchie, R. H. Plasma Losses by Fast Electrons in Thin Films. *Phys. Rev.* **1957**, *106*, 874–881.
2. Barnes, W. L.; Dereux, A.; Ebbesen, T. W. Surface Plasmon Subwavelength Optics. *Nature* **2003**, *424*, 824–830.
3. Haes, A. J.; Haynes, C. L.; McFarland, A. D.; Schatz, G. C.; Van Duyne, R. P.; Zou, S. Plasmonic Materials for Surface-Enhanced Sensing and Spectroscopy. *MRS Bull.* **2005**, *30*, 368–375.
4. Lal, S.; Link, S.; Halas, N. J. Nano-optics from Sensing to Waveguiding. *Nat. Photonics* **2007**, *1*, 641–648.
5. Polman, A. Plasmonics Applied. *Science* **2008**, *322*, 868–869.
6. Mansuripur, M.; Zakharian, A. R.; Lesuffleur, A.; Oh, S. H.; Jones, R. J.; Lindquist, N. C.; Im, H.; Kobyakov, A.; Moloney, J. V. Plasmonic Nano-Structures for Optical Data Storage. *Opt. Express* **2009**, *17*, 14001–14014.
7. Ebbesen, T. W.; Lezec, H. J.; Ghaemi, H. F.; Thio, T.; Wolff, P. A. Extraordinary Optical Transmission Through Subwavelength Hole Arrays. *Nature* **1998**, *391*, 667–669.
8. Genet, C.; Ebbesen, T. W. Light in Tiny Holes. *Nature* **2007**, *445*, 39–46.
9. Brolo, A. G.; Gordon, R.; Leathem, B.; Kavanagh, K. L. Surface Plasmon Sensor Based on the Enhanced Light Transmission through Arrays of Nanoholes in Gold Films. *Langmuir* **2004**, *20*, 4813–4815.
10. Stark, P. R. H.; Halleck, A. E.; Larson, D. N. Short Order Nanohole Arrays in Metals for Highly Sensitive Probing of Local Indices of Refraction as the Basis for a Highly Multiplexed Biosensor Technology. *Methods* **2005**, *37*, 37–47.
11. Stewart, M. E.; Mack, N. H.; Malyarchuk, V.; Soares, J.; Lee, T. W.; Gray, S. K.; Nuzzo, R. G.; Rogers, J. A. Quantitative Multispectral Biosensing and 1D Imaging Using Quasi-3D Plasmonic Crystals. *Proc. Natl. Acad. Sci. U.S.A.* **2006**, *103*, 17143–17148.
12. Tetz, K. A.; Pang, L.; Fainman, Y. High-Resolution Surface Plasmon Resonance Sensor Based on Linewidth-Optimized Nanohole Array Transmittance. *Opt. Lett.* **2006**, *31*, 1528–1530.
13. Pang, L.; Hwang, G. M.; Slutsky, B.; Fainman, Y. Spectral Sensitivity of Two-Dimensional Nanohole Array Surface Plasmon Polariton Resonance Sensor. *Appl. Phys. Lett.* **2007**, *91*, 123112.
14. Gordon, R.; Sinton, D.; Kavanagh, K. L.; Brolo, A. G. A New Generation of Sensors Based on Extraordinary Optical Transmission. *Acc. Chem. Res.* **2008**, *41*, 1049–1057.
15. Yang, J. C.; Ji, J.; Hogle, J. M.; Larson, D. N. Metallic Nanohole Arrays on Fluoropolymer Substrates as Small Label-Free Real-Time Bioprobes. *Nano Lett.* **2008**, *8*, 2718–2724.
16. Im, H.; Lesuffleur, A.; Lindquist, N. C.; Oh, S. H. Plasmonic Nanoholes in a Multichannel Microarray Format for Parallel Kinetic Assays and Differential Sensing. *Anal. Chem.* **2009**, *81*, 2854–2859.
17. Ferreira, J.; Santos, M. J. L.; Rahman, M. M.; Brolo, A. G.; Gordon, R.; Sinton, D.; Girotto, E. M. Attomolar Protein Detection Using in-Hole Surface Plasmon Resonance. *J. Am. Chem. Soc.* **2009**, *131*, 436–437.
18. Lindquist, N. C.; Lesuffleur, A.; Im, H.; Oh, S. H. Submicron Resolution Surface Plasmon Resonance Imaging Enabled by Nanohole Arrays with Surrounding Bragg Mirrors for Enhanced Sensitivity and Isolation. *Lab Chip* **2009**, *9*, 382–387.
19. Williams, S. M.; Rodriguez, K. R.; Teeters-Kennedy, S.; Stafford, A. D.; Bishop, S. R.; Lincoln, U. K.; Coe, J. V. Use of the Extraordinary Infrared Transmission of Metallic Subwavelength Arrays to Study the Catalyzed Reaction of Methanol to Formaldehyde on Copper Oxide. *J. Phys. Chem. B* **2004**, *108*, 11833–11837.
20. Coe, J. V.; Heer, J. M.; Teeters-Kennedy, S.; Tian, H.; Rodriguez, K. R. Extraordinary Transmission of Metal Films with Arrays of Subwavelength Holes. *Annu. Rev. Phys. Chem.* **2008**, *59*, 179–202.
21. Chan, G. H.; Zhao, J.; Schatz, G. C.; Van Duyne, R. P. Localized Surface Plasmon Resonance Spectroscopy of Triangular Aluminum Nanoparticles. *J. Phys. Chem. C* **2008**, *112*, 13958–13963.
22. Gao, H. W.; Henzie, J.; Lee, M. H.; Odom, T. W. Screening Plasmonic Materials Using Pyramidal Gratings. *Proc. Natl. Acad. Sci. U.S.A.* **2008**, *105*, 20146–20151.
23. Love, J. C.; Estroff, L. A.; Kriebel, J. K.; Nuzzo, R. G.; Whitesides, G. M. Self-Assembled Monolayers of Thiolates on Metals as a Form of Nanotechnology. *Chem. Rev.* **2005**, *105*, 1103–1169.
24. Ferry, V. E.; Sweatlock, L. A.; Pacifici, D.; Atwater, H. A. Plasmonic Nanostructure Design for Efficient Light Coupling into Solar Cells. *Nano Lett.* **2008**, *8*, 4391–4397.

25. Lindquist, N. C.; Luhman, W. A.; Oh, S. H.; Holmes, R. J. Plasmonic Nanocavity Arrays for Enhanced Efficiency in Organic Photovoltaic Cells. *Appl. Phys. Lett.* **2008**, *93*, 123308.
26. George, S. M.; Ott, A. W.; Klaus, J. W. Surface Chemistry for Atomic Layer Growth. *J. Phys. Chem.* **1996**, *100*, 13121–13131.
27. Groner, M. D.; Fabreguette, F. H.; Elam, J. W.; George, S. M. Low-Temperature Al_2O_3 Atomic Layer Deposition. *Chem. Mater.* **2004**, *16*, 639–645.
28. Groner, M. D.; George, S. M.; McLean, R. S.; Carcia, P. F. Gas Diffusion Barriers on Polymers Using Al_2O_3 Atomic Layer Deposition. *Appl. Phys. Lett.* **2006**, *88*, 051907.
29. Whitney, A. V.; Elam, J. W.; Zou, S. L.; Zinovev, A. V.; Stair, P. C.; Schatz, G. C.; Van Duyne, R. P. Localized Surface Plasmon Resonance Nanosensor: A High-Resolution Distance-Dependence Study Using Atomic Layer Deposition. *J. Phys. Chem. B* **2005**, *109*, 20522–20528.
30. Zhang, X. Y.; Zhao, J.; Whitney, A. V.; Elam, J. W.; Van Duyne, R. P. Ultrastable Substrates for Surface-Enhanced Raman Spectroscopy: Al_2O_3 Overlayers Fabricated by Atomic Layer Deposition Yield Improved Anthrax Biomarker Detection. *J. Am. Chem. Soc.* **2006**, *128*, 10304–10309.
31. Barnes, W. L.; Murray, W. A.; Dintinger, J.; Devaux, E.; Ebbesen, T. W. Surface Plasmon Polaritons and Their Role in the Enhanced Transmission of Light through Periodic Arrays of Subwavelength Holes in a Metal Film. *Phys. Rev. Lett.* **2004**, *92*, 107401.
32. Gao, H. W.; Henzie, J.; Odom, T. W. Direct Evidence for Surface Plasmon-Mediated Enhanced Light Transmission through Metallic Nanohole Arrays. *Nano Lett.* **2006**, *6*, 2104–2108.
33. Genet, C.; van Exter, M. P.; Woerdman, J. P. Fano-Type Interpretation of Red Shifts and Red Tails in Hole Array Transmission Spectra. *Opt. Commun.* **2003**, *225*, 331–336.
34. Jung, L. S.; Campbell, C. T.; Chinowsky, T. M.; Mar, M. N.; Yee, S. S. Quantitative Interpretation of the Response of Surface Plasmon Resonance Sensors to Adsorbed Films. *Langmuir* **1998**, *14*, 5636–5648.
35. Przybilla, F.; Degiron, A.; Laluet, J. Y.; Genet, C.; Ebbesen, T. W. Optical Transmission in Perforated Noble and Transition Metal Films. *J. Opt. A* **2006**, *8*, 458–463.
36. Krishnan, A.; Thio, T.; Kima, T. J.; Lezec, H. J.; Ebbesen, T. W.; Wolff, P. A.; Pendry, J.; Martin-Moreno, L.; Garcia-Vidal, F. J. Evanescently Coupled Resonance in Surface Plasmon Enhanced Transmission. *Opt. Commun.* **2001**, *200*, 1–7.
37. Stewart, M. E.; Yao, J. M.; Maria, J.; Gray, S. K.; Rogers, J. A.; Nuzzo, R. G. Multispectral Thin Film Biosensing and Quantitative Imaging Using 3D Plasmonic Crystals. *Anal. Chem.* **2009**, *81*, 5980–5989.
38. Chinowsky, T. M.; Mactutis, T.; Fu, E.; Yager, P. Optical and Electronic Design for a High-Performance Surface Plasmon Resonance Imager. *Proc. SPIE* **2004**, *5261*, 173–182.
39. Park, S. H. K.; Oh, J.; Hwang, C. S.; Lee, J. I.; Yang, Y. S.; Chu, H. Y. Ultrathin Film Encapsulation of an OLED by ALD. *Electrochem. Solid State Lett.* **2005**, *8*, H21–H23.
40. Rezania, A.; Johnson, R.; Lefkow, A. R.; Healy, K. E. Bioactivation of Metal Oxide Surfaces. 1. Surface characterization and Cell Response. *Langmuir* **1999**, *15*, 6931–6939.
41. Wu, X. H.; Sun, Y. G.; Pelton, M. Recombination Rates for Single Colloidal Quantum Dots Near a Smooth Metal Film. *Phys. Chem. Chem. Phys.* **2009**, *11*, 5867–5870.
42. Nagpal, P.; Lindquist, N. C.; Oh, S. H.; Norris, D. J. Ultrasmooth Patterned Metals for Plasmonics and Metamaterials. *Science* **2009**, *325*, 594–597.
43. Henzie, J.; Lee, M. H.; Odom, T. W. Multiscale Patterning of Plasmonic Metamaterials. *Nat. Nanotechnol.* **2007**, *2*, 549–554.
44. Haynes, C. L.; Van Duyne, R. P. Nanosphere Lithography: A Versatile Nanofabrication Tool for Studies of Size-Dependent Nanoparticle Optics. *J. Phys. Chem. B* **2001**, *105*, 5599–5611.
45. Lee, S. H.; Bantz, K. C.; Lindquist, N. C.; Oh, S.-H.; Haynes, C. L. Self-Assembled Plasmonic Nanohole Arrays. *Langmuir* **2009**, *25*, 13685–13693.
46. Johnson, P. B.; Christy, R. W. Optical Constants of the Noble Metals. *Phys. Rev. B* **1972**, *6*, 4370–4379.